Article:
He, X, Tian, F, Bai, X et al. (3 more authors) (2020) Biomimetic lubricant-infused titania nanoparticle surfaces via layer-by-layer deposition to control biofouling. Applied Surface Science, 515. 146064. ISSN 0169-4332

https://doi.org/10.1016/j.apsusc.2020.146064

Biomimetic lubricant-infused titania nanoparticle surfaces via layer-by-layer deposition to control biofouling

Xiaoyan He [a,b], Feng Tian [a], Xiuqin Bai [a,&], Chengqing Yuan [a], Chun Wang [b], Anne Neville [b]

[a] Reliability Engineering Institute, National Engineering Research Center for Water Transport Safety, Wuhan University of Technology, Wuhan 430063, China

[b] Institute of Functional Surfaces, School of Mechanical Engineering, University of Leeds, Leeds LS2 9JT, United Kingdom

[&] Corresponding author.

E-mail address: xqbai@whut.edu.cn

ABSTRACT

Lubricant-infused surfaces have attracted a lot of attention in antifouling applications. Previously, lubricant-infused surfaces fabricated by a layer-by-layer process involved two or more polyelectrolytes and needed post-treatments to generate pores. Here, the paper proposes a layer-by-layer sol-gel process to prepare a lubricant-infused surface. This process only involves a single material and without any post-treatment. The nanostructured titania layers were layer-by-layer assembled onto 316L stainless steel substrates by immersing the substrates into a titanium (IV) butoxide ethanol solution. The titania layers were subsequently surface-functionalized by fluorinated silanes and infiltrated with fluorinated lubricant to form lubricant-infused nanoparticle surfaces. The physicochemical properties of the lubricant-infused nanoparticle surfaces dominated the antifouling performance. These results give some insight into the construction of lubricant-infused nanoparticle surfaces with desirable liquid repellency and antifouling properties via a layer-by-layer sol-gel process.

KEYWORDS：lubricant-infused; nanoparticle surface; layer-by-layer sol-gel process; wettability; antifouling

1. Introduction

Liquid-repellent surfaces widely exist in nature, including the lotus leaf [1], gecko feet [2], cicada wings [3], butterfly wings [4], and rice leaves [4]. Superhydrophobic surfaces have developed rapidly in the last decade [5-7]. Liquid droplets can easily roll off the superhydrophobic surface and take away contaminants. Superhydrophobic surfaces therefore occupy an important position in antifouling applications. However, inherent limitations of superhydrophobic surfaces severely restrict their applications. First, the air layers cannot stand up to pressure, humidity, and biological fluids [8-11]. Moreover, the air layers are not stable in an underwater environment. For example, superhydrophobic surfaces often cannot have long term antifouling performance in a marine environment.

Nature has provided a remarkably simple alternative approach. The Nepenthes pitcher plant overcomes the shortcomings of superhydrophobic surfaces. For the Nepenthes pitcher plant, an intermediary liquid layer is locked by its rough surface to act as a repellent surface. Inspired by this, Wong et al. [12] proposed liquid-repellent surfaces, which were called as “Slippery Liquid Infused Porous Surfaces” (SLIPSs). SLIPSs have attracted a lot of attention owing to their great liquid repellency [13, 14] and antifouling performances [15]. Wong et al. [12] proposed three principles for constructing stable SLIPSs: (1) the solid surface must have a micro/nano rough structure to provide a large surface to entrap and lock liquid lubricant, (2) the solid surface must prefer to entrap the liquid lubricant instead of the repellent liquid and (3) the liquid lubricant is immiscible with the repellent liquid.

The micro/nano rough structures on solid substrates are necessary to prepare SLIPSs. At present, numerous techniques have been used to construct micro/nano rough structures for SLIPSs, including femtosecond laser direct writing [16, 17], reactive ion etching [18], photolithography [19], electrochemical deposition [8], sol-gel [20], and so on. These methods are complicated and require specific equipment. Layer-by-layer assembly provides a simple solution to form a porous surface [10]. It is a convenient method which can be performed at ambient temperature and pressure. Moreover, layer-

by-layer assembly could adjust surface structures at the micro and nanoscales according to the sizes of polyelectrolytes and assembly conditions. SLIPSs were previously successfully created by layer-by-layer assembly with polyelectrolytes [10, 21, 22]. Sunny et al. [10] used layer-by-layer deposition with positively charged polydiallyldimethylammonium chloride and negatively charged silica nanoparticles to create a nanostructured surface. The structured surface was further modified by fluorinated silanes and infused with lubricant to form a SLIPS with highly antifouling properties. Manabe et al. [23] prepared a SLIPS by layer-by-layer assembly deposition with silica nanoparticles and chitin nanofibers. Moreover, Manabe et al. [24] prepared a mix layer-by-layer film, which contributed to the electrostatic interactions between positively charged chitosan and negatively charged alginate as well as the hydrogen-bonding between alginate and polyvinylpyrrolidone (PVPON). After the components in the mixed film were cross-linked, the PVPON in the film was removed to obtain porosity to fabricate a SLIPS. The as-prepared SLIPS showed great potential as a nonfouling material. All these studies usually involved two or more polyelectrolytes in the layer-by-layer process and required post-treatments to remove one polyelectrolyte to generate the porosity for liquid lubricant. Layer-by-layer self-assembly deposition to construct a porous structure with a simpler approach would bring great benefit and this work presents a self-assembly approach via a single material.

Up to now, there was no report about the porous nanostructure on a SLIPS which was formed via layer-by-layer sol-gel process of alkoxide. The hydrolysis of alkoxide could form nanoparticles to generate a porous structure [25]. Compared with the layer-by-layer assembly of polyelectrolytes, in-situ hydrolysis of alkoxide is more flexible to construct porous structures at the micro and nanoscales. Firstly, the nanopores can be controlled by the reaction conditions in the hydrolysis process, without being limited by the original particle sizes of polyelectrolytes. Moreover, the porous nanostructures can be constructed directly without extra post-treatment. The layer-by-layer sol-gel deposition process of alkoxide to construct porous nanostructures for SLIPSs is novel and offers the possibility to radically simplify the porous layer synthesis.

Stainless steels are widely used in marine environments for their superior mechanical properties and high corrosion resistance [8]. However, stainless steesl are still troubled by biofouling. Herein, we report construction of SLIPSs on stainless steel substrates by a simple layer-by-layer sol-gel process of alkoxide for antifouling applications. A nanostructured layer formed by titania nanoparticles was layer-by-layer assembled onto a given substrate by immersing the substrate into an ethanol solution containing titanium (IV) butoxide. The titania nanoparticle layer, formed by the hydrolysis of titanium (IV) butoxide with abundant hydroxyl, was further modified by fluorinated silanes and resulted in enough space to entrap liquid lubricant. This method allows us to fabricate a SLIPS with desirable antiwetting and antifouling properties by a layer-by-layer sol-gel process.

2. Experimental section

2.1. Materials

316L stainless steel (SS, nominal composition of 0.029 wt.% C, 0.075 wt.% N, 0.71 wt.% Si, 0.035 wt.% P, 2.04 wt.% Mo, 0.02 wt.% S, 15.92 wt.% Cr, 1.41 wt.% Mn, 11.35 wt.% Ni and remaining iron) was used. The (1H,1H,2H,2H-perfluorodecyl)-triethoxysilane (PFTEOS, Sigma-Aldrich, 96%) was used as received. DuPont Krytox GPL 100 lubricant with a density of 1870 kg/m^3 at 0 °C and a surface tension of 17±1 mN/m was used as lubricant.

2.2. Fabrication

The 316L stainless steel substrates (10 mm × 10 mm × 2 mm) were polished and then washed sequentially in acetone, ethanol and water. Subsequently, the clean substrates were soaked into a piranha solution (95-97% sulfuric acid and 30% hydrogen peroxide in 7:3 volumetric ratio) for 30 minutes to clean the surfaces and generate hydroxyl groups (denoted as SS−OH). After piranha solution treatment, samples were washed by deionized water and subsequently drying. The titania multilayer was deposited on the SS−OH surface via the layer-by-layer sol-gel process. In brief, the SS−OH surface was soaked into 0.1 M titanium (IV) butoxide ethanol solution for 10 minutes. The hydroxyl

groups on the SS−OH surface induce the hydrolysis reaction of titanium (IV) butoxide. The samples were rinsed in ethanol three times to remove the unreacted alkoxides and then soaked in deionized water for 2 minutes to recreate the hydroxyl groups on titania particles (Ti−OH). They were then dried. The steps were repeated several times to produce titania layers (denoted as SS−TiO_2).

The SS−TiO_2 samples were immersed into a 1 vol % PFTEOS ethanol solution for 1 h at 37 °C and then transferred into an oven for 1 h at 120 °C to make sure that the PFTEOS molecules completely chemically bind to the multilayer (denoted as SS−TiO_2−F). Then, lubricant was added drop by drop onto the modified sample. After the lubricant was spread onto the whole surface, the samples were tilted vertically for more than 12 h to remove the excess lubricant (denoted as SS−TiO_2−S).

2.3. Characterization

Microstructural features of the samples were examined by field emission scanning electron microscopy (FESEM, Zeiss Ultra Plus, Germany). The topography of the samples was characterized by atomic force microscopy (AFM, Bruker Dimension FastScan^{TM}) and the roughness was obtained by the equipped NanoScope Analysis software (Bruker). The chemical components of samples were analyzed using X-ray photoelectron spectroscopy (XPS, ESCALAB 250Xi, U.S.A) with radiation resource of Al-k_α (1486.6 eV).

The wettability of these surfaces was tested by a contact angle meter (Dataphysics OCA 15EC, Germany) at room temperature. The static water contact angles (CA) were determined from deionized water with a droplet of 3 μL. The CA data were acquired using ellipse fitting. Water contact angle hysteresis (CAH) was calculated by the difference between advancing contact angle (ACA) and receding contact angle (RCA). The ACA was measured in the process of increasing the volume of a drop of deionized water and the RCA was measured in the process of decreasing the volume of a drop of deionized water by an image analysis system. Each test was repeated in triplicate.

2.4. Antifouling performance

A marine strain of *Phaeodactylum tricornutum* was typically selected in this work. The adhesion behavior of *P. tricornutum* on samples was used to assess their antifouling performance. The adhesion experiments were conducted in sterilized artificial seawater (ASW) which was prepared according to ASTM D1141-98. *P. tricornutum* was cultured in sterilized Guillard's F/2 growth medium with 0.03 g/L $Na_2SiO_3 \cdot 9H_2O$. The algae were cultured at 20 °C in an illumination incubator with a 12 h: 12 h light/dark cycle.

The algal suspension with a concentration of 5×10^6 cells/mL was prepared. The samples were soaked in the algal suspension and incubated for 7 days at 20 °C in an illumination incubator with a 12 h:12 h light/dark cycle. After incubation, the samples were washed with sterilized ASW to remove unadhered algae and then fixed by 2.5% glutaraldehyde for 2 h. The adhesion behavior of *P. tricornutum* was observed by confocal laser scanning microscopy (CLSM, Leica TCS SP8, Germany). CLSM pictures were further quantified using the COMSTAT program to obtain a series of biofilm parameters to characterize the features of biofilms formed on different samples [26]. Each test was repeated in triplicate.

3. Results and Discussion

3.1. The fabrication process of nanoscale coatings

The fabrication process of the SLIPS is shown in Fig. 1. A porous layer was formed by a layer-by-layer sol-gel deposition process of titanium (IV) butoxide. The process comprised chemisorption and hydrolysis of titanium (IV) butoxide (Fig. 1a-d) [25]. In detail, hydroxyl groups were generated on the substrate by immersion in a piranha solution. A piranha solution is usually used to create hydroxyl groups on stainless steel substrates [27]. The substrate was subsequently immersed into a titanium (IV) butoxide ethanol solution. Titanium (IV) butoxide was chemisorbed on the hydroxylated surface by the hydrolysis reaction of the $Ti{-}O{-}(CH_2)_3CH_3$ with the surface hydroxyl groups [27] (Fig. 1b). The surfaces with chemisorbed alkoxide were then rinsed in deionized

water to cause the hydrolysis of the chemisorbed alkoxides, resulting the formation of titania nanoparticles and regeneration of hydroxyl groups (Fig. 1c) [28]. The regenerated hydroxyl groups continued to induce the chemisorption of alkoxide when the samples were again put in the titanium (IV) butoxide ethanol solution. The chemisorption and hydrolysis steps were repeated to produce a porous titania layer assembly on the substrate (Fig. 1d). The titania layer was subsequently modified by PFTEOS to produce a fluorinated surface. The silane molecules of PFTEOS were strongly anchored to the hydroxylated surface by reaction of the hydrolysis silane species ($Si{-}O{-}CH_2CH_3$) with the surface functional groups ($Ti{-}OH$) to form a self-assembled monolayer with low surface energy (Fig. 1e). A fluorinated lubricant oil was then infused into the porous nanostructure to create a lubricant layer, thus forming a SLIPS (Fig. 1f).

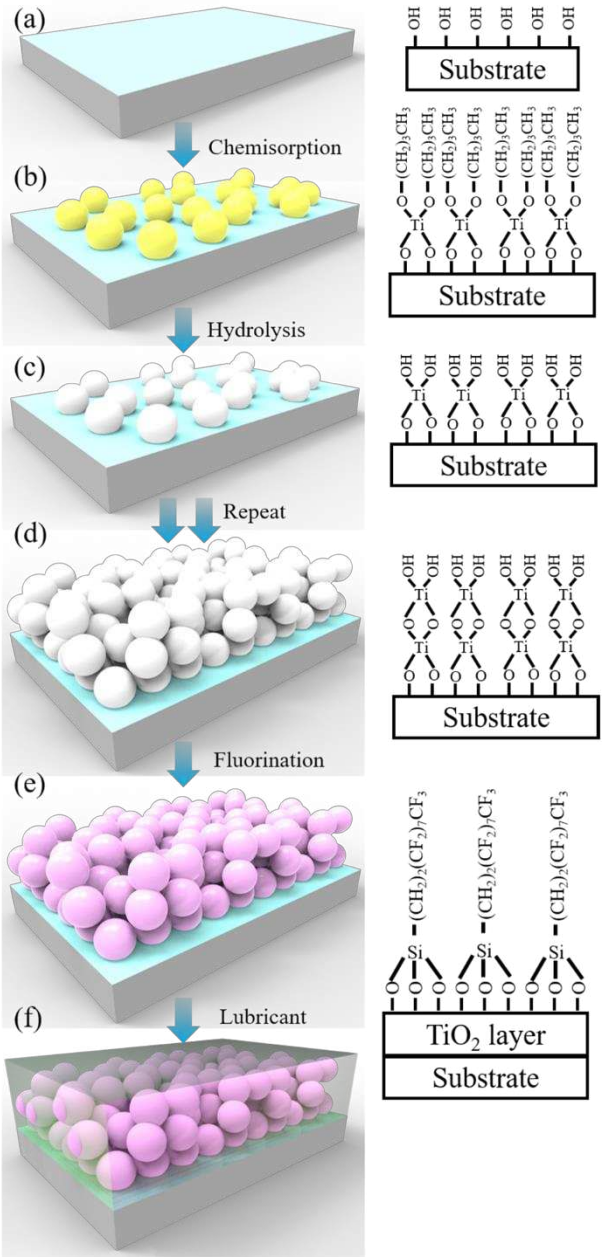

Fig. 1. Schematic view of the layer-by-layer sol-gel deposition process to form a lubricant-infused porous surface. Hydroxyl groups were generated on the substrate (a) and subsequent chemisorption (b) and hydrolysis (c) of titanium (IV) butoxide to form a nanostructured titania multilayer (d). After the surface was covalently functionalized with PFTEOS (e), a liquid lubricant was infused into the nanostructured layer (f), forming a SLIPS.

3.2. Characterization of the as-prepared layers

The chemical composition of the as-prepared surface was characterized by XPS

analysis. The Ti *2p* spectrum acquired from the as-prepared surface is presented in Fig. 2a. In the Ti *2p* spectral region, there are two peaks at 459.1 eV and 464.7 eV, which are assigned to TiO_2 $2p_{3/2}$ and TiO_2 $2p_{1/2}$ peaks, respectively [29]. A shoulder on the high-binding-energy side is contributed to their satellite peak. The symmetric shape and satellite feature indicate the successful formation of titania particles. The O 1s spectrum acquired from the as-prepared surface, is resolved into two components, namely TiO_2 (529.6 eV) [29], and C−O (531.2 eV) (Fig. 2b). These results indicate that the as-prepared layer is composed of titania particles.

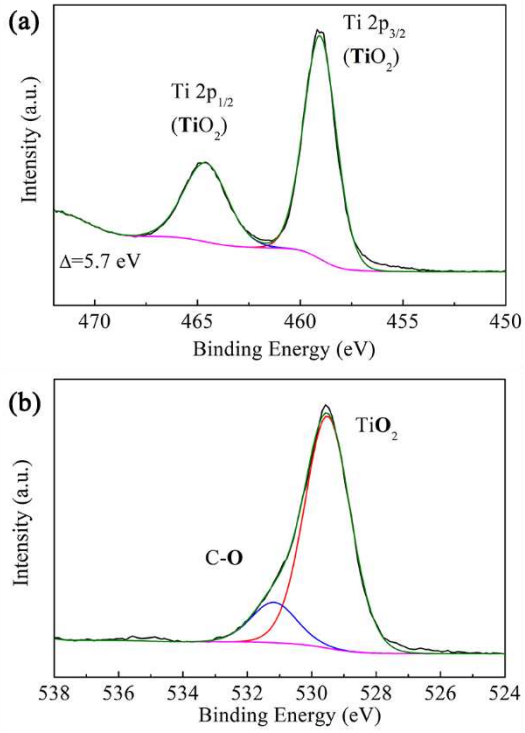

Fig. 2. High-resolution XPS spectra of Ti *2p* (a) and O *1s* (b) detected from the as-prepared surface.

SEM images of the titania layers on stainless steel substrates prepared with different deposition cycles are shown in Fig. 3, indicating that titania multilayers are successfully established on the stainless steel substrates. The titania layer after one deposition cycle is compact with ~ 26 nm nanoparticles, resulting in a nano-porous structure. The titania layer after three deposition cycle exhibits an obvious micro/nano-porous structure. The bottom layer has ~ 26 nm nanoparticles and the upper layer has ~ 50 nm nanoparticles. The titania nanoparticles and their aggregates result in a micro/nano-porous structure with ~ 40 nm nanopores and ~ 1 μm micro-grooves after 5 deposited cycles. With an increased number of deposition cycles, the nano-porous structure replaces the

micro/nano-porous structure. Titania particles with sizes of ~ 50 nm are exhibited on all these coatings, suggesting the particle sizes are independent of the number of deposition cycles.

AFM images of the titania layers on stainless steel prepared with different deposition cycles were also characterized (Fig. 3). The SS−OH surface is very smooth and the root mean square roughness (RMS) is about 1.82 nm (5 μm×5 μm) (Fig. 3 a-3). The titania layer after one deposition cycle exhibits a little rougher surface with RMS of 5.77 nm (5 μm×5 μm) (Fig. 3 b-3). For other titania layers, the RMS is significantly increased to 30.7 nm, 26.4 nm and 26.0 nm, respectively. The titania layer after three deposition cycles and the titania layer after five deposition cycles are a little rougher than the titania layer after seven deposition cycles, which agrees with SEM observations. The height distribution of nanoparticles on the surface increases at beginning and then slightly decreases, indicating that the surface becomes uniform with increased deposition cycles. The surface morphologies and roughness are changed after different number of deposition cycles. This allows the surface morphology, roughness and thickness of the coating to be controlled by varying the number of deposition cycles.

A porous nanostructure is preferred to form an encapsulated configuration, which is beneficial to the stability of samples [30]. The titania layer after seven deposition cycles can supply enough space to entrap the lubricant and the lubricant can be stable stored by the capillary force induced by their nano-porous structure. Therefore, the titania layer after seven deposition cycles with a porous nanostructure is used for the rest of the study.

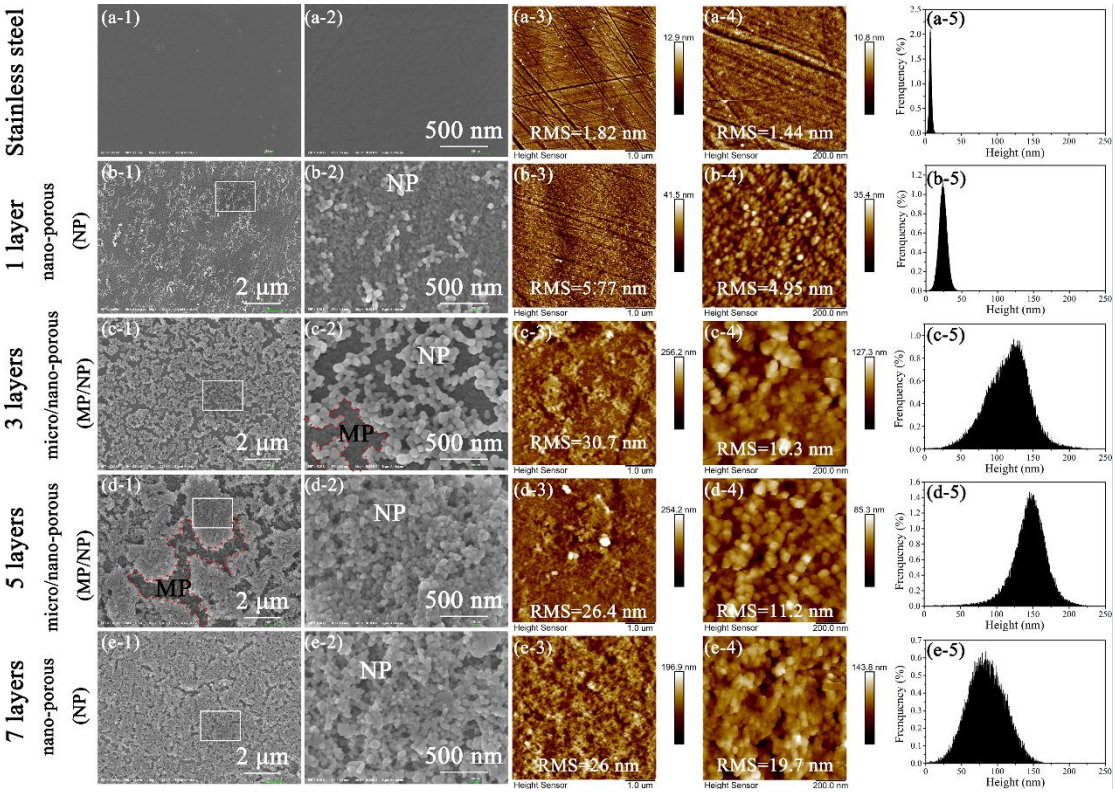

Fig. 3. SEM images (1-2) and AFM images (3-5) of the surface topographies after different deposition cycles on stainless steel substrates: without deposition (a), 1 layer (b), 3 layers (c), 5 layers (d) and 7 layers (e). -2 is the high magnification view of -1, respectively. -4 is the high magnification view of -3, respectively. -5 is the height distribution of -3, respectively.

3.4. Characterization of the fluorinated and lubricant-infused surfaces

The surface-functionalized process with fluorinated silanes is necessary to form a stable lubricant-infused surface [30]. The titania surface was first chemically modified by PFTEOS to ensure that the solid was preferred to be wetted by lubricant (Fig. S1). XPS spectra results demonstrate that PFTEOS molecules are successfully bound with the titania layer (Fig. 4). PFTEOS can bind with the hydroxylated titania surface by the hydrolysis process to form a fluorinated titania surface (Fig. S2). Subsequently, the lubricant is spread on the top of the fluorinated surface (Fig. 4). Capillary forces mainly contribute to the retention of the lubricant on the nano-porous titania surface, since the diameter of the pores is much lower than ~1 mm which is the capillary length of the lubricant under Earth's gravity [31]. Meanwhile, the van der Waals forces also benefit

the storage of the liquid lubricant [15].

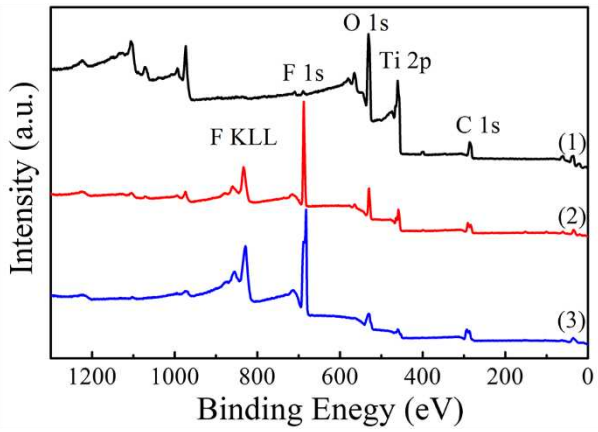

Fig. 4. XPS spectra of the SS−TiO_2 (1), SS−TiO_2−F (2) and SS−TiO_2−S (3) surfaces.

3.5. Wettability

The wettability of different surfaces was quantified by a contact angle meter. The SS−OH, SS−TiO_2, SS−TiO_2−F, SS−TiO_2−S surfaces exhibit different CA and CAH values (Fig. 5). Table 1 presents their CAs and surface free energies (γ) which were calculated by the Owens-Wendt-Rabel-Kaelble (OWRK) method using three kinds of test liquids: water, glycol, and diiodomethane.

The SS−OH surface shows a water CA of 50.7 ± 4.8°, which is smaller than the water CA of native stainless steel, indicating that the SS−OH surface is more hydrophilic. The surface energy reveals a polar contribution (γ^p) of 20.47 mN/m. It leads to significant fouling on SS−OH, since the high polar contribution of surface free energy usually results in serious biofouling of biomacromolecules [17]. The water remains on the surface even though it is at 180° tilt. This strong adhesion between water and the substrate can contribute to the hydrogen bond between water and hydroxyl groups on stainless steel, further indicating the enrichment of hydroxyl groups on the SS−OH surface.

The SS−TiO_2 surface is superhydrophilic with a water CA of 0°, where the water droplet is almost not visible (Fig. 5b). This superhydrophilicity could contribute to the hydrogen bond between water and the hydroxyl groups on titania layers (Ti−OH).

Indeed, the presence of porosity on titania layers can facilitate water to spread onto the surface through capillary forces.

The SS−TiO_2−F surface was then characterized. Water contact angle measurement indicates that the fluorosilanization was successfully achieved, as the SS−TiO_2−F surface presents a sharp increase in water CA compared with the SS−TiO_2 surface (155.6 ± 0.5° versus 0°). The synergistic effect of surface chemistry and surface structure results in its superhydrophobicity. Meanwhile, an extremely low CAH (0.5 ± 0.1°) is observed on the SS−TiO_2−F surface and the liquid droplet easily rolls off from the SS−TiO_2−F surface. The high water CA and the low CAH indicate that the SS−TiO_2−F surface was in a suspended Cassie-Baxter's state [7]. The porosity in the titania nanoparticle layer is mainly responsible for this phenomenon, where the air layer entrapped by the porous layer effectively prevents the penetration of water into the surface. However, the air layer cannot prevent the spread of liquids with low surface tension. The lubricant CA of SS−TiO_2−F surface is nearly 0° (Fig. S1). Fluorosilanization is therefore performed to provide affinity to liquid lubricant to guarantee the stability of lubricant-infused surfaces [12]. Otherwise, the lubricant would be displaced by water (Fig. 5 e,f). The fluorosilanization is necessary in the formation of a stable SS−TiO_2−S surface.

Lubricant infusion shows a great impact on surface wettability. An obvious decrease in water CA occurs on the SS−TiO_2−S surface compared with the SS−TiO_2−F surface (120.9 ± 2.5° versus 155.6 ± 0.5°). The phenomenon can be explained by the formation of a liquid lubricant interface. There are two kinds of lubricant infusion states, namely the encapsulated state and the impregnated-emerged state [17]. If the lubricant is in the encapsulated state, the lubricant covers all over the surface (Fig. 6). While the lubricant only infuses in the cavities if the lubricant is in the impregnated-emerged state (Fig. 6). A low CAH usually occurs on the surface when it is in the encapsulated state [17, 30]. Dynamic goniometry evidence that the SS−TiO_2−S surface presents an extremely low CAH value (1.9 ± 1.4°). Therefore, the SS−TiO_2−S surface is in the encapsulated state

with a smooth liquid interface. Meanwhile, the surface energy of SS−TiO_2−S surface is about 14.93 mN/m (Table 1), which also indicates the lubricant is covered on the surface, as it is close to the lubricant surface tension (17 ± 1 mN/m).

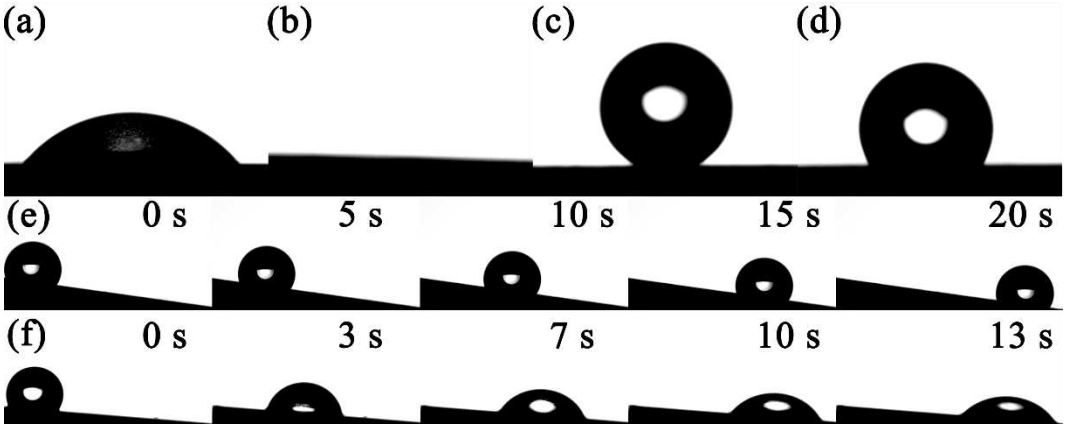

Fig. 5. Water droplets on the SS−OH (a), SS−TiO_2 (b), SS−TiO_2−F (c), SS−TiO_2−S (d) surfaces, Evaluation of the stability of lubricant layers on the fluorinated (e) and non-fluorinated (f) SS−TiO_2 surfaces.

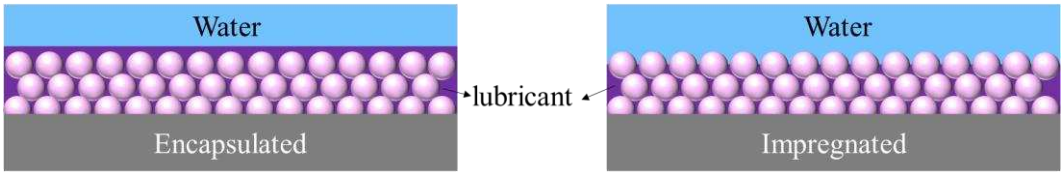

Fig. 6. Possible water-lubricant-solid configurations for liquid-infused surfaces.

Table 1 CAs and surface energies of different samples

	Water CA (deg)	Glycol CA (deg)	Diiodomethane CA (deg)	γ^{tot} (mN/m)	γ^{d} (mN/m)	γ^{p} (mN/m)
SS−OH	50.7 ± 4.8	23.4 ± 0.5	48.4 ± 1.7	51.76	31.29	20.47
SS−TiO_2	0	0	0	Impossible to determine [a]		
SS−TiO_2−F	155.6 ± 0.5	120.8 ± 1.	124.1 ± 3.2	Impossible to determine [a]		
SS−TiO_2−S	120.9 ± 2.5	95.9 ± 0.4	91.2 ± 0.5	14.93	14.78	0.15

[a] Surface energy was calculated from CAs of three liquids. It is difficult to calculate the surface energy of the SS−TiO_2 and SS−TiO_2−F surfaces since that the observed CAs resulted from their surface morphology and surface energy.

3.6. Antifouling performance

Antifouling performance of these surfaces after incubation in *P. tricornutum* suspension for 7 days is shown in Fig. 7. The surface properties greatly influence the antifouling performance of samples by comparing their adhesion ratio. Adhesion ratio is defined as the ratio of adhesion area of *P. tricornutum* to total surface area of substratum [32]. The SS−TiO_2 surface has poor antifouling properties with an obvious increase (126%) in fouling compared with the SS−OH reference. The antifouling performance is observed on the SS−TiO_2−F surface, presenting a slight decrease (12%) in fouling compared with the SS−OH reference. The best antifouling performance is observed on the SS−TiO_2−S surface, with a significant decrease (97%) in fouling compared with the SS−OH reference.

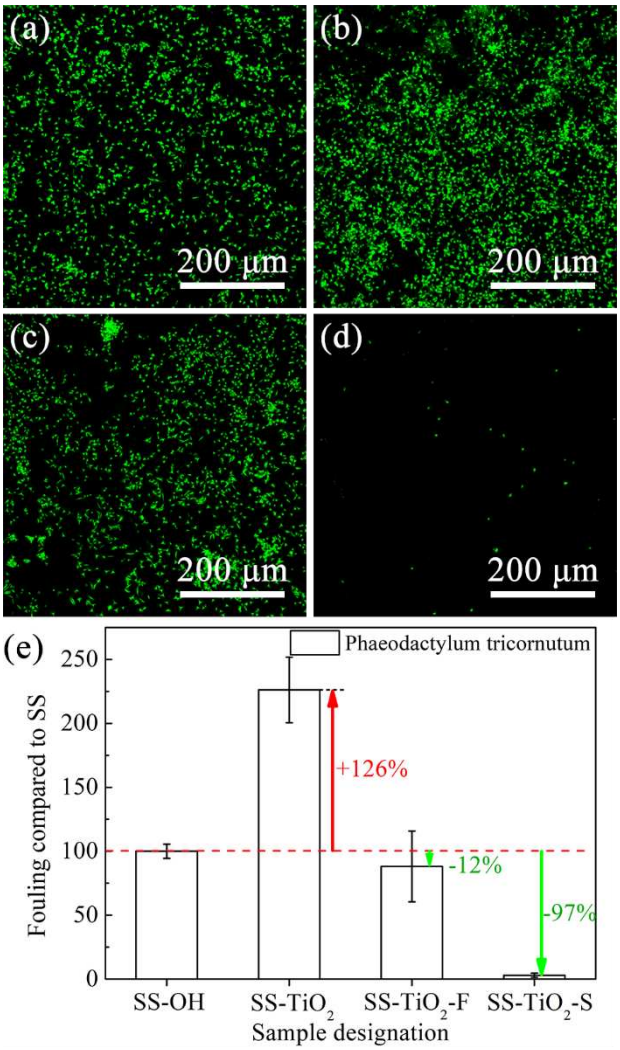

Fig. 7. CLSM images of adhered *P. tricornutum* on the SS−OH (a), SS−TiO_2 (b),

SS−TiO_2−F (c), and SS−TiO_2−S (d) surfaces. Antifouling performance to *P. tricornutum* of the different surfaces compared with the SS−OH reference (e).

CLSM images were further analyzed by the COMSTAT program to obtain key biofilm parameters to elucidate the biofilm formation on different surfaces. The results showed that total biomass of the biofilm dramatically increased (267%) on the SS−TiO_2 surface and decreased (98%) on the SS−TiO_2−S surface compared with the SS−OH reference (Fig. 8a). Compared with the biofilm grown on the SS−OH reference, the average thickness was significantly higher (281%) for the biofilm grown on the SS−TiO_2 surface and lower (98%) for biofilm grown on the SS−TiO_2−S surface (Fig. 8b). The total biomass of the biofilm grown on the SS−TiO_2−F surface presented a decrease (45%) compared with the SS−OH reference. The average thickness was also decreased by 33%. The total biomass and the average thickness gave a more obvious antifouling performance of the SS−TiO_2−F surface compared with the adhesion ratio. The results also indicated that the SS−TiO_2−S possessed the best antifouling property.

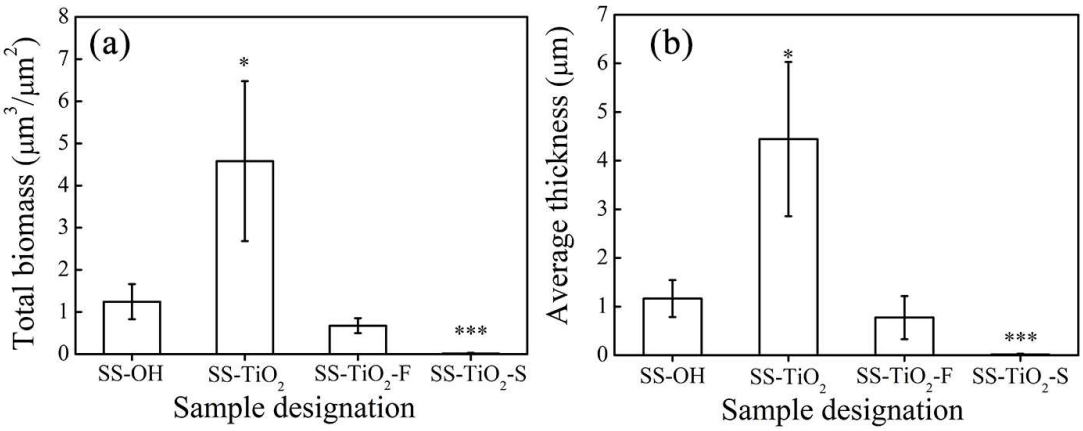

Fig. 8. The key parameters of *P. tricornutum* biofilm on different samples: total biomass (a), average thickness (b). * $p < 0.05$ and *** $p < 0.01$, as compared with biofilm grown on the SS−OH reference.

Factors, including surface topography, surface wettability and surface chemistry, have impact on antifouling performances [30, 32]. It is speculated that the hydrophilicity is the main reason responsible for the worst antifouling performance of the SS−TiO_2 surface. The titania layers formed by the sol-gel method are hydroxylated. It is common knowledge that the hydrophilic surfaces possess good biofouling resistance [32, 33].

While these observations are normally related to hydrophilic nature of polymers or hydrogels, where water molecules can get together to produce a hydration layer, acting as a barrier to resist foulants [32]. However, the SS−TiO_2 surface, which is a superhydrophilic metallic oxide, does not belong to the phenomenon. The superhydrophilic SS−TiO_2 surface leads to a high surface energy, resulting in serious biofouling [17]. When comparing the fouling results on the SS−TiO_2 and SS−TiO_2−F surfaces, it appears that the SS−TiO_2−F surface has a positive impact on antifouling performance, as the SS−TiO_2−F surface shows much less adhesion of *P. tricornutum* than that on the SS−TiO_2 surface. Meanwhile, the SS−TiO_2−F surface can effectively decrease the biomass and thickness of biofilm (Fig. 8 a,b). The antifouling performance of the SS−TiO_2−F surface is related to its wettability. The SS−TiO_2−F surface is in a suspended Cassie-Batxter's state. In this state, the SS−TiO_2−F surface can resist biofouling by the air layer entrapped in the rough structure. Some proteins secreted by *P. tricornutum* can destroy the suspended Cassie-Baxter's state of the SS−TiO_2−F surface [17]. As a result, the self-cleaning properties of the SS−TiO_2−F surface are not significant as we expected. The SS−TiO_2−S surface provides a much better solution. The antifouling performance of the SS−TiO_2−S surface is excellent, and could decrease biofilm formation by 98%. The SS−TiO_2−S surface is in the encapsulated state (Fig. 5). In this state, the lubricant layer can isolate the microorganisms from the targeted solid surface to effectively decrease biofouling [34]. Our attempt to fabricate the lubricant-infused titania coatings provides the feasibility of SLIPSs fabrication by layer-by-layer sol-gel deposition process. Meanwhile, the protocols by layer-by-layer sol-gel deposition process can be expected to fabricate lubricant-infused surfaces with different substrate materials, shapes and sizes.

4. Conclusions

A simple process was developed to introduce a lubricant-infused surface on stainless steel. The nanostructure was formed via a layer-by-layer sol-gel deposition process of titanium (IV) butoxide. The in-situ hydrolysis of titanium (IV) butoxide was flexible to construct a nano-porous structure and generate abundant hydroxyl to be further

modified by fluorinated silanes. After fluorosilanization, a liquid lubricant was infused into the porous nanoparticle layer. The strong affinity of the lubricant to the substrate ensured stability of the lubricant-infused surface. The lubricant-infused titania surface resulted in successful resistance to water and foulants. This method allows us to fabricate lubricant-infused nanoscale coatings with desirable antiwetting and antifouling properties by layer-by-layer sol-gel deposition process.

Conflicts of interest

The authors declare no competing financial interest.

Acknowledgments

This work was supported by the International Postdoctoral Exchange Fellowship Program (No. 20190060), China Postdoctoral Science Foundation (No. 2017M622542), Hubei Postdoctoral Sustentation Foundation, China (No. G22), and Foundation of Key Laboratory of Marine Materials and Related Technologies, Ningbo Institute of Materials Technology and Engineering, Chinese Academy of Sciences (No. 2018K07).

References

[1] L. Jiang, Y. Zhao, J. Zhai, A lotus-leaf-like superhydrophobic surface: A porous microsphere/nanofiber composite film prepared by electrohydrodynamics, Angew. Chem. Int. Ed. 43 (2004) 4338-4341.

[2] S. Ma, Q. Ye, X. Pei, D. Wang, F. Zhou, Antifouling on gecko's feet inspired fibrillar surfaces: evolving from land to marine and from liquid repellency to algae resistance, Adv. Mater. Interfaces 2 (2015) 1500257.

[3] E.P. Ivanova, J. Hasan, H.K. Webb, V.K. Truong, G.S. Watson, J.A. Watson, V.A. Baulin, S. Pogodin, J.Y. Wang, M.J. Tobin, C. Löbbe, R.J. Crawford, Natural bactericidal surfaces: mechanical rupture of pseudomonas aeruginosa cells by cicada wings, Small 8 (2012) 2489-2494.

[4] G.D. Bixler, A. Theiss, B. Bhushan, S.C. Lee, Anti-fouling properties of

microstructured surfaces bio-inspired by rice leaves and butterfly wings, J. Colloid Interface Sci. 419 (2014) 114-133.

[5] S. Nishimoto, B. Bhushan, Bioinspired self-cleaning surfaces with superhydrophobicity, superoleophobicity, and superhydrophilicity, RSC Adv. 3 (2013) 671-690.

[6] B. Zhang, J. Li, X. Zhao, X. Hu, L. Yang, N. Wang, Y. Li, B. Hou, Biomimetic one step fabrication of manganese stearate superhydrophobic surface as an efficient barrier against marine corrosion and Chlorella vulgaris-induced biofouling, Chem. Eng. J. 306 (2016) 441-451.

[7] X. He, P. Cao, F. Tian, X. Bai, C. Yuan, Autoclaving-induced in-situ grown hierarchical structures for construction of superhydrophobic surfaces: A new route to fabricate antifouling coatings, Surf. Coat. Tech. 357 (2019) 180-188.

[8] A.B. Tesler, P. Kim, S. Kolle, C. Howell, O. Ahanotu, J. Aizenberg, Extremely durable biofouling-resistant metallic surfaces based on electrodeposited nanoporous tungstite films on steel, Nat. Commun. 6 (2015).

[9] C. Shillingford, N. MacCallum, T.S. Wong, P. Kim, J. Aizenberg, Fabrics coated with lubricated nanostructures display robust omniphobicity, Nanotechnology 25 (2014) 014019.

[10] S. Sunny, N. Vogel, C. Howell, T.L. Vu, J. Aizenberg, Lubricant-infused nanoparticulate coatings assembled by layer-by-layer deposition, Adv. Funct. Mater. 24 (2014) 6658-6667.

[11] M. Liu, Y. Hou, J. Li, L. Tie, Z. Guo, Transparent slippery liquid-infused nanoparticulate coatings, Chem. Eng. J. 337 (2018) 462-470.

[12] T.S. Wong, S.H. Kang, S.K.Y. Tang, E.J. Smythe, B.D. Hatton, A. Grinthal, J. Aizenberg, Bioinspired self-repairing slippery surfaces with pressure-stable omniphobicity, Nature 477 (2011) 443-447.

[13] C. Howell, T.L. Vu, C.P. Johnson, X. Hou, O. Ahanotu, J. Alvarenga, D.C. Leslie, O. Uzun, A. Waterhouse, P. Kim, M. Super, M. Aizenberg, D.E. Ingber, J. Aizenberg, Stability of surface-immobilized lubricant interfaces under flow, Chem. Mater. 27 (2015) 1792-1800.

[14] X. Gao, Z. Guo, Mechanical stability, corrosion resistance of superhydrophobic steel and repairable durability of its slippery surface, J. Colloid Interface Sci. 512 (2018) 239-248.

[15] S. Amini, S. Kolle, L. Petrone, O. Ahanotu, S. Sunny, C.N. Sutanto, S. Hoon, L. Cohen, J.C. Weaver, J. Aizenberg, N. Vogel, A. Miserez, Preventing mussel adhesion using lubricant-infused materials, Science 357 (2017) 668-673.

[16] J. Yong, F. Chen, Q. Yang, Y. Fang, J. Huo, J. Zhang, X. Hou, Nepenthes inspired design of self-repairing omniphobic slippery liquid infused porous surface (SLIPS) by femtosecond laser direct writing, Adv. Mater. Interfaces 4 (2017).

[17] S. Zouaghi, T. Six, S. Bellayer, S. Moradi, S.G. Hatzikiriakos, T. Dargent, V. Thomy, Y. Coffinier, C. Andre, G. Delaplace, M. Jimenez, Antifouling biomimetic liquid-infused stainless steel: application to dairy industrial processing, ACS Appl. Mater. Interfaces 9 (2017) 26565-26573.

[18] J. Wang, K. Kato, A.P. Blois, T.S. Wong, Bioinspired omniphobic coatings with a thermal self-repair function on industrial materials, ACS Appl. Mater. Interfaces 8 (2016) 8265-8271.

[19] I. You, T.G. Lee, Y.S. Nam, H. Lee, Fabrication of a micro-omnifluidic device by omniphilic/omniphobic patterning on nanostructured surfaces, ACS Nano 8 (2014) 9016-9024.

[20] P. Kim, M.J. Kreder, J. Alvarenga, J. Aizenberg, Hierarchical or not? Effect of the length scale and hierarchy of the surface roughness on omniphobicity of lubricant-infused substrates, Nano Lett. 13 (2013) 1793-1799.

[21] S. Sunny, G. Cheng, D. Daniel, P. Lo, S. Ochoa, C. Howell, N. Vogel, A. Majid, J. Aizenberg, Transparent antifouling material for improved operative field visibility in endoscopy, Proc. Natl. Acad. Sci. 113 (2016) 11676-11681.

[22] X. He, F. Tian, X. Bai, C. Yuan, Role of trapped air and lubricant in the interactions between fouling and SiO_2 nanoparticle surfaces, Colloids Surf. B 184 (2019) 110502.

[23] K. Manabe, S. Nishizawa, K.-H. Kyung, S. Shiratori, Optical phenomena and

antifrosting property on biomimetics slippery fluid-infused antireflective films via layer-by-layer comparison with superhydrophobic and antireflective films, ACS Appl. Mater. Interfaces 6 (2014) 13985-13993.

[24] K. Manabe, K.-H. Kyung, S. Shiratori, Biocompatible slippery fluid-infused films composed of chitosan and alginate via layer-by-layer self-assembly and their antithrombogenicity, ACS Appl. Mater. Interfaces 7 (2015) 4763-4771.

[25] I. Izumi, S. Hiroyuki, K. Toyoki, Stepwise adsorption of metal alkoxides on hydrolyzed surfaces : a surface sol-gel process, Chem. Lett. 25 (1996) 831-832.

[26] A. Heydorn, A.T. Nielsen, M. Hentzer, C. Sternberg, M. Givskov, B.K. Ersbøll, S. Molin, Quantification of biofilm structures by the novel computer program COMSTAT, Microbiology 146 (2000) 2395-2407.

[27] S.J. Yuan, S.O. Pehkonen, Y.P. Ting, K.G. Neoh, E.T. Kang, Inorganic-organic hybrid coatings on stainless steel by layer-by-layer deposition and surface-initiated atom-transfer-radical polymerization for combating biocorrosion, ACS Appl. Mater. Interfaces 1 (2009) 640-652.

[28] J. Borges, J.F. Mano, Molecular interactions driving the layer-by-layer assembly of multilayers, Chem. Rev. 114 (2014) 8883-8942.

[29] J. Peyre, V. Humblot, C. Methivier, J.M. Berjeaud, C.M. Pradier, Co-grafting of amino poly(ethylene glycol) and Magainin I on a TiO_2 Surface: tests of antifouling and antibacterial activities, J. Phys. Chem. B 116 (2012) 13839-13847.

[30] X. He, P. Cao, F. Tian, X. Bai, C. Yuan, Infused configurations induced by structures influence stability and antifouling performance of biomimetic lubricant-infused surfaces, Surf. Coat. Tech. 358 (2019) 159-166.

[31] P. Wang, D. Zhang, Z. Lu, S. Sun, Fabrication of slippery lubricant-infused porous surface for inhibition of microbially influenced corrosion, ACS Appl. Mater. Interfaces 8 (2016) 1120-1127.

[32] X. He, X. Suo, X. Bai, C. Yuan, H. Li, Functionalizing aluminum substrata by quaternary ammonium for antifouling performances, Appl. Surf. Sci. 440 (2018) 300-307.

[33] D.Y. Zhang, Q. Hao, J. Liu, Y.S. Shi, J. Zhu, L. Su, Y. Wang, Antifouling polyimide membrane with grafted silver nanoparticles and zwitterion, Sep. Purif. Technol. 192 (2018) 230-239.

[34] J. Yin, M.L. Mei, Q. Li, R. Xia, Z. Zhang, C.H. Chu, Self-cleaning and antibiofouling enamel surface by slippery liquid-infused technique, Sci. Rep. 6 (2016) 25924.